Astronomy & Astrophysics manuscript no. template
June 1, 2023

A Theoretical Prediction of the CMB Power Spectrum

J. A. Glenndal

Institute of Theoretical Astrophysics, University of Oslo, 0315 Oslo, Norway
e-mail: j.a.glenndal@astro.uio.no

June 01, 2023

ABSTRACT

We calculated the CMB power spectrum following the paper of Callin (2006). The calculations were divided into four milestones, where we first solved the background universe, followed by the recombination history of the universe. We then calculated the perturbation history of the universe, using linear perturbation theory, and finally the CMB power spectrum using the line of sight integration approach to get the photon temperature multipoles, Θ_ℓ, at all Fourier scales, k, evaluated today. For the cosmological parameters, we used the Planck 2018 best fits, but we removed neutrinos, since we do not perturb them. We found that the power spectrum had peaks corresponding to compressions and decompressions in the plasma that existed before recombination where the hydrogen atom formed and the universe became transparent. The first four peaks were located between $\ell \sim 10^2$ and $\ell \sim 10^3$. For larger ℓ we observed photon diffusion. For smaller ℓ we compared our result to data and observed that our results are consistent with observations.

Key words. cosmic microwave background (CMB) – large-scale structure of Universe

1. Introduction

The CMB power spectrum can tell us a lot about the universe. Since the universe is homogeneous and isotropic on large scales, the Friedmann-Lemaître-Robertson-Walker line element describes the geometry in our universe. From this metric, one can use the well known Friedmann equations to calculate the time evolution of the energy components and the expansion history of the universe. As the power spectrum will change with these parameters, one can in principle use the observed power spectrum to constrain the energy components of the universe today. Further, the power spectrum tells us about recombination. This is possible since the power spectrum is length scale dependent, and perturbations created sound waves in the plasma that travelled until recombination, where the plasma became neutral. The sound waves then froze out and left a detectable imprint scale on the photon temperature field. There is much more to learn from the power spectrum.

In milestone 1 we look at the background universe, and discuss the results. In milestone 2 we look at more closely at recombination and the evolution of the free electron density in the universe. In milestone 3 we use linear perturbation theory to perturb the Einstein and Boltzmann equations. These coupled differential equations are solved numerically and the solution is discussed. In the last milestone, everything is put together, and we present the matter and CMB power spectra.
The paper of Callin (2006) and the web page of Winther (2023) were especially useful for the calculation of the CMB power spectrum.

2. Milestone I

In this milestone we look at the expansion history of a homogeneous and isotropic universe governed by the well known Friedmann equation 3. The universe we consider consists of baryonic matter (Ω_b), cold dark matter (Ω_{CDM}), radiation (Ω_γ), neutrinos (Ω_ν) and dark energy (Ω_Λ), where Ω is the mass/energy density divided by the critical density ($\rho_c = 3H^2/8\pi G$).

We calculate the time evolution of several important quantities that we will need later. For instance, the expansion history is important to know, since the redshift of the CMB photons measured today is dependent on how fast the universe has expanded during the journey of the photons. Further, the background solution will in later milestones be perturbed to obtain a solution for the perturbations that existed during the release of the CMB photons. These perturbations will change the energy of the photons, since some photons had to climb out of the potential well created by the perturbations.

2.1. Theory

The parameters we use for our universe are given below.

$$
\begin{aligned}
h &= 0.67,\\
T_{\text{CMB0}} &= 2.7255\ K,\\
N_{\text{eff}} &= 3.046,\\
\Omega_{\text{b0}} &= 0.05,\\
\Omega_{\text{CDM0}} &= 0.267,\\
\Omega_{k0} &= 0,\\
\Omega_{\nu 0} &= N_{\text{eff}} \cdot \frac{7}{8}\left(\frac{4}{11}\right)^{4/3} \Omega_{\gamma 0},\\
\Omega_{\gamma 0} &= 2 \cdot \frac{\pi^2}{30}\frac{(k_b T_{\text{CMB0}})^4}{\hbar^3 c^5} \cdot \frac{8\pi G}{3H_0^2},\\
\Omega_{\Lambda 0} &= 1 - (\Omega_{k0} + \Omega_{b0} + \Omega_{\text{CDM0}} + \Omega_{\gamma 0} + \Omega_{\nu 0}),
\end{aligned}
\tag{1}
$$

where the subscript 0 denotes today's value. h is the dimensionless Hubble constant. More details can be found at Winther (2023).

The geometry of a flat, isotropic and homogeneous universe expressed in comoving spherical coordinates with cosmic time, t, is given by the Friedmann-Lemaître-Robertson-Walker (FLRW) metric seen in equation 2.

$$ds^2 = -c^2dt^2 + a^2(t)\left(dr^2 + r^2(d\theta^2 + \sin^2\theta d\phi^2)\right) \tag{2}$$

The Friedmann equation is given by

$$H = H_0\sqrt{(\Omega_{b0} + \Omega_{\text{CDM0}})a^{-3} + (\Omega_{\gamma 0} + \Omega_{\nu 0})a^{-4} + \Omega_{k0}a^{-2} + \Omega_{\Lambda 0}}, \tag{3}$$

where a is the scale factor and $H = \frac{\dot{a}}{a}$. We will not use cosmic time, t, as our time variable. Instead, we use $x = \ln a$ as our dimensionless time variable. This implies that $a = e^x$ for conversion. Since $a(t = 0) = 0$ and $a(t = t_0) = 1$ we get $t = 0 \iff x = -\infty$ and $t = t_0 \iff x = 0$. The cosmic time as a function of x be found from the differential equation

$$\frac{dt}{dx} = \frac{1}{H}, \tag{4}$$

which can be solved numerically. The equation will be solved from the radiation dominated era until today. The initial condition is therefore given by $t(x_{\text{start}}) = \frac{1}{2H(x_{\text{start}})}$. We also define the scaled Hubble parameter defined by $\mathcal{H} \equiv aH$, which will often occur in later equations. The conformal time, η, measured in length, as another time variable. This quantity is the comoving distance light has travelled since the big bang, and after inflation it is strictly increasing with time. For photons travelling radially in a flat universe, the FLRW metric tells us that the comoving distance, η, light has travelled in cosmic time, t, is given by

$$\frac{d\eta}{dt} = \frac{c}{a}. \tag{5}$$

Using substitutions, we get that

$$\frac{d\eta}{dx} = \frac{c}{\mathcal{H}}, \tag{6}$$

which can be solved numerically using $\eta(x_{\text{start}}) = \frac{c}{\mathcal{H}(x_{\text{start}})}$.

The evolution of the Ωs can be expressed as a function of a as showed below.

$$\begin{aligned}
\Omega_k(a) &= \frac{\Omega_{k0}}{a^2H(a)^2/H_0^2} \\
\Omega_{\text{CDM}}(a) &= \frac{\Omega_{\text{CDM0}}}{a^3H(a)^2/H_0^2} \\
\Omega_b(a) &= \frac{\Omega_{b0}}{a^3H(a)^2/H_0^2} \\
\Omega_\gamma(a) &= \frac{\Omega_{\gamma 0}}{a^4H(a)^2/H_0^2} \\
\Omega_\nu(a) &= \frac{\Omega_{\nu 0}}{a^4H(a)^2/H_0^2} \\
\Omega_\Lambda(a) &= \frac{\Omega_{\Lambda 0}}{H(a)^2/H_0^2}.
\end{aligned} \tag{7}$$

The luminosity distance is given by $d_L = \frac{r}{a}$, where r is the comoving distance light has travelled between some source and us, given by

$$r = \begin{cases} \chi \cdot \frac{\sin(\sqrt{|\Omega_{k0}|}H_0\chi/c)}{(\sqrt{|\Omega_{k0}|}H_0\chi/c)} & \Omega_{k0} < 0 \\ \chi & \Omega_{k0} = 0 \\ \chi \cdot \frac{\sinh(\sqrt{|\Omega_{k0}|}H_0\chi/c)}{(\sqrt{|\Omega_{k0}|}H_0\chi/c)} & \Omega_{k0} > 0, \end{cases}$$

where $\chi = \eta(x = 0) - \eta(x)$.

Lastly, to find the best fit parameters of our universe, we can compare our theoretical model to supernova data, d_L^{obs}. In equation 8 z is the redshift and σ is the uncertainty. We sample different χ^2 values using Metropolis MCMC.

$$\chi^2(h, \Omega_{m0}, \Omega_{k0}) = \sum_{i=1}^{N} \frac{[(d_L(z_i, h, \Omega_{m0}, \Omega_{k0}) - d_L^{\text{obs}}(z_i)]^2}{\sigma_i^2} \tag{8}$$

2.2. Implementation details

The code needs h, Ω_B, Ω_{CDM}, Ω_K, N_{eff} and T_{CMB} to run. The differential equations are solved using a Runge-Kutta 4 ODE solver, and the result was splined using a cubic spline. We solve from $x = -20$ until $x = 5$ with 1000 points linearly spaced.

2.3. Results

2.4. Testing the code

In figure 1 we see that the code produces the expected results when comparing to the plots in Winther (2023). The time of radiation matter equality is shown in table 1, and takes the value of $x = -8.13$. The time of matter dark energy equality is at $x = -0.26$. When looking at the plots, we see that the results take the expected analytical values around the correct times.

2.5. Our results

In figure 2 we show a plot of the conformal Hubble parameter, $\mathcal{H}(x)$, which will often appear in calculations. $\mathcal{H}(x)$ is in actuality just $\dot{a}$, i.e. the rate of which the scale factor changes with respect to x. For two galaxies following the Hubble flow, the comoving distance, d_{comoving}, is constant and equal to the physical distance today, since $d = a \cdot d_{\text{comoving}}$. The rate of change in the distance between them, v, is simply $v = \dot{a} \cdot d_{\text{comoving}} = \mathcal{H}d_{\text{comoving}} = Hd$, which is the Hubble law. Since we study the FLRW universe, we know that massive particles follow the Hubble flow, so v tells us firstly that at any given time, particles will move away from us twice as fast if they are twice as far away. Secondly, $\mathcal{H}(x)$ is, at any given time, the constant of proportionality for the first relation. In other words, $\mathcal{H}(x)$ is the expansion rate of the universe. In the plot, we see that this rate was largest at early times. We also see that the slope changes around radiation matter equality and around matter dark energy equality. This can be understood by solving the Friedmann equation with one energy density component at a time. When dark energy becomes more dominant in the total energy density of the universe, the universe start to expand more rapidly again. This is because the mass density has become too low for mass to be bound by "gravity". This happens at some time before matter dark energy equality as we can see in the table 1.

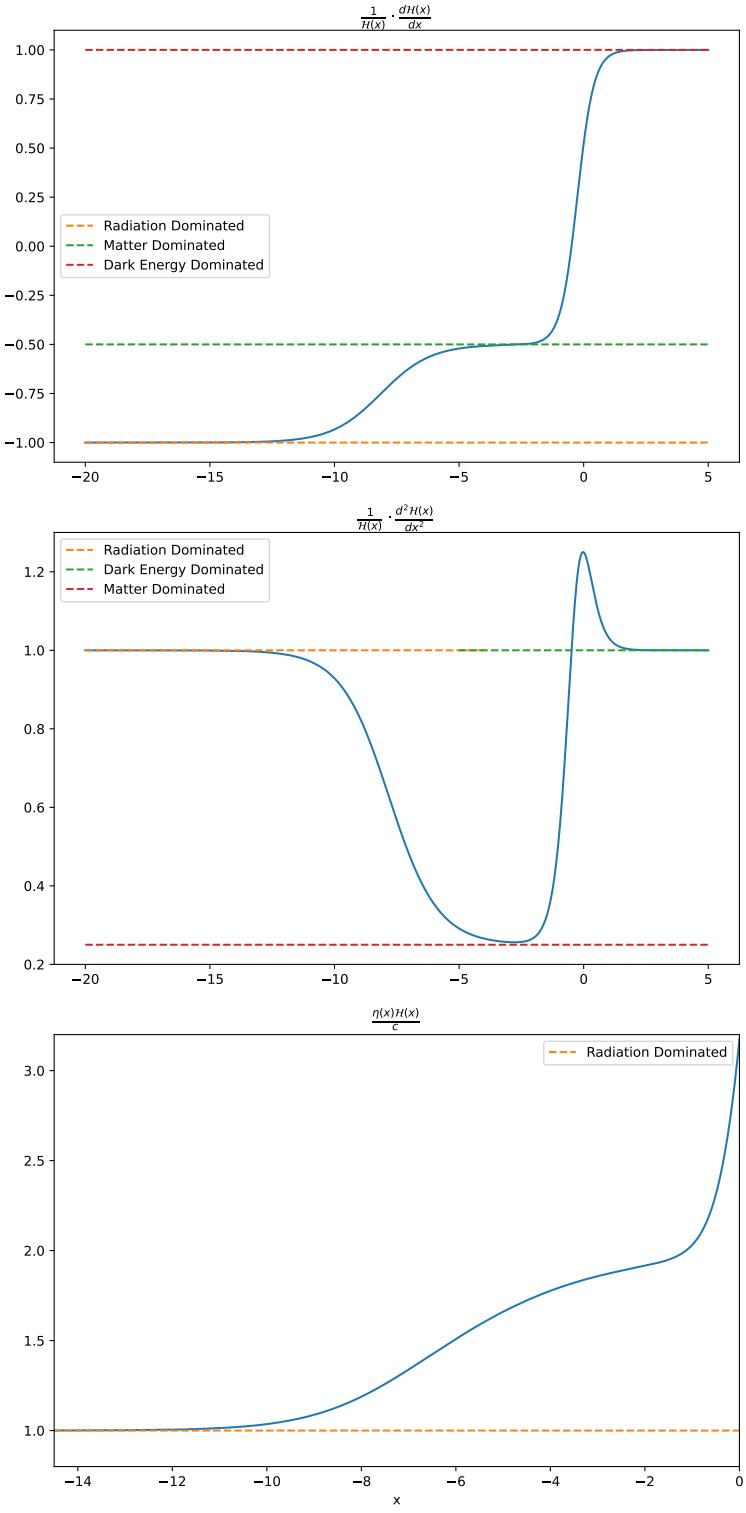

Fig. 1. Plots to demonstrate that the code works properly. The dotted lines are the theoretical predictions.

In figure 3 we see the cosmic time, which is the time measured by an observer following the Hubble flow, plotted against x. The scale factor is proportional to $t^{1/2}$ during radiation domination, and proportional to $t^{2/3}$ during matter domination, Scott Dodelson (2021). This explains why there is a change in the slope around radiation matter equality. As expected, the time today is of order giga years.

Table 1. Important times in cosmology stated in x, z and t.

Event	x, z, t
Radiation-Matter equality	-8.13, 3400.33, 51.06 [10^3 yr]
Matter-Dark energy equality	-0.26, 0.29, 10.38 [Gyr]
Time of cosmic acceleration	-0.49, 0.63, 7.76 [Gyr]
Age of the universe today	0.00, 0.00, 13.86 [Gyr]
Conformal time today	1.90, -0.85, 46.32 [Gyr]

In figure 4 we see the conformal time, $\eta(x)$. The conformal time, measured in length, is the distance light could have travelled, in comoving coordinates, since the big bang. Measured in time, η is then the amount of time light would have used to travel η in length. The conversion factor between time and length is the speed of light. Since $a = 1$ today, $\eta(0)$ is then the size of the observable universe today, since light could have travelled those distances since the big bang. $\eta(x)$ is the comoving distance of causality. The physical distance of causality at cosmic time, t, is then $a(t) \cdot \eta(x(t))$. The conformal time, in time, is larger than the cosmic time since the universe has expanded. The expansion made all distances larger, and if we freeze the expansion, light would need more than 13.8 billion years to travel across the radius of the observable universe. From table 1 we see that light would need 46.3 billion years to travel this distance. Again we see that the slope changes around radiation matter equality, which is related to the change in $\mathcal{H}$. The physical reason for why η can change with respect to the cosmic time, is that the scale factor changes with time. If the scale factor is constant, η will grow linearly. If the universe expands with the speed of light everywhere, η will be constant, since light will not move relative to the comoving coordinates.

In figure 5 we see how much each energy density parameter contributes to the sum of the energy density parameters. We see that the dark energy component remains a small part of the total energy density in the universe until recently relative to the age of the universe. In the future, dark energy will be the only relevant density parameter, so the universe will expand faster in the future compared to today. In the radiation dominated era, the universe was dominated by relativistic particles. As the universe expanded and cooled down, the particles lost energy, and the energy content was dominated by non-relativistic matter. As the universe continued to expand, the mass density decreases with the scale factor in all three spatial dimensions, i.e. $\rho \propto \frac{1}{a^3}$. Since the cosmological constant is constant everywhere, the total amount of dark energy must increase when more space is created. This is observed close to $x = 0$ in the plot.

In figure 6 we see that our model of the universe predicts a luminosity distance curve that agrees reasonably well with observations. This suggests that the universe is close to being flat. In figure 7 we see the 1σ and 2σ constraints from MCMC fits to supernova data in the Ω_Λ vs. Ω_M plane. The average value of the small Hubble parameter was $h = 0.70$ with $1\sigma = 0.0064$. We allowed curvature when fitting the data, and our best fit suggests, with $\chi^2 = 29.28$, that the curvature density parameter, Ω_K, is equal to 0.11.

In table 1 we show some times for different events in the universe.

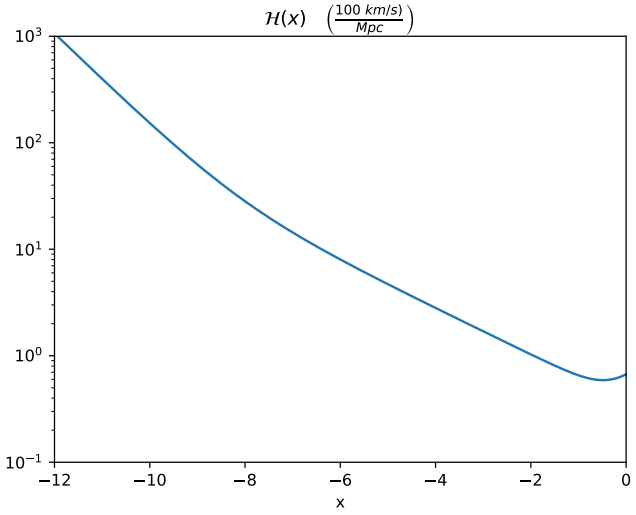

Fig. 2. The conformal Hubble parameter as a function of x.

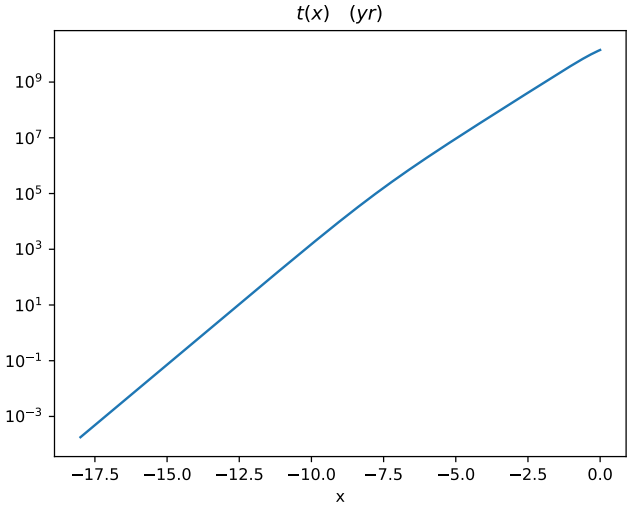

Fig. 3. The cosmic time as a function of x.

3. Milestone II

When the photon temperature in the universe became too low for photons to ionize the hydrogen atom, a period of recombination begun in the universe. In this period, neutral hydrogen started to form, and the free electron density decreased. This led to a dramatic change in the scattering rate of light, since photons scatter on free electrons. After this period, light could travel mostly freely towards us. These photons are the CMB photons that we in the end wish to study.

The aim of this milestone is to calculate the optical depth for photons emitted at time x observed by us today, and the visibility function. More details on these functions later.

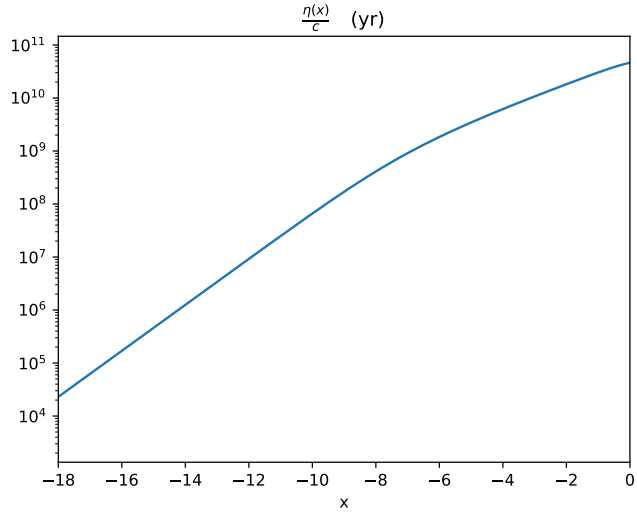

Fig. 4. The conformal time as a function of x.

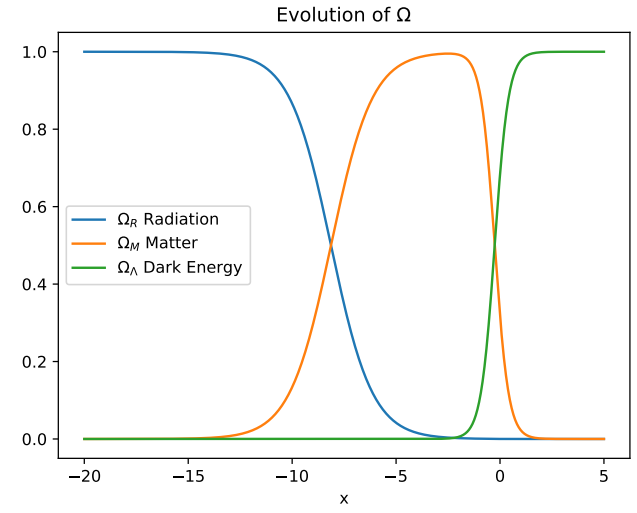

Fig. 5. The density parameters as a function of x.

3.1. Theory

The photon intensity can decrease when photons travel through a medium. This can be due to Thomson scattering, where photons interact with free electrons and the direction of propagation changes. For an initial intensity I_0, the resulting intensity at any given displacement from the origin, y, inside the medium can be described by

$$I(y) = I_0 e^{-\tau(y)}, \tag{9}$$

where $\tau(y)$ is the optical depth as a function of y. Since intensity is a conserved quantity if light travels unimpeded, the optical depth can tell us how much of the initial intensity that has been lost due to processes in the medium, e.g. scattering. τ is defined by

$$\tau(\eta) = \int_{\eta}^{\eta_0} n_e(\eta')\sigma_T a(\eta') d\eta', \tag{10}$$

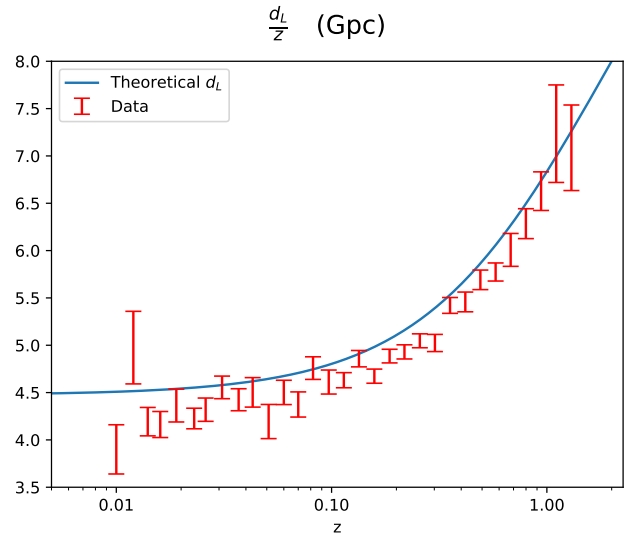

Fig. 6. The theoretical luminosity distance, divided by redshift, is plotted against redshift. Actual data from supernova observations is overplotted.

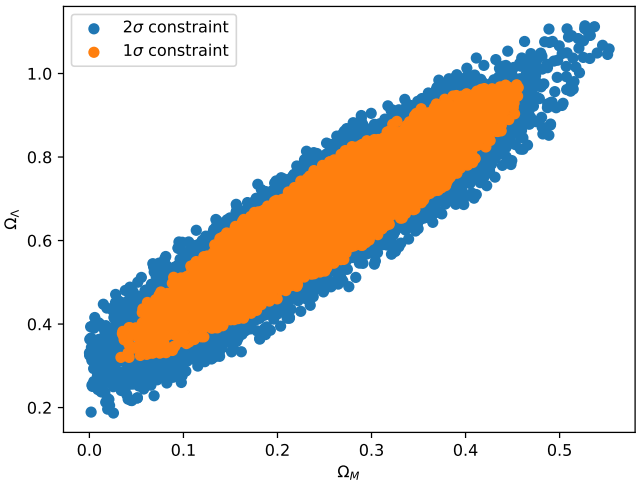

Fig. 7. The 1σ and 2σ constraints from MCMC fits to supernova data in the Ω_Λ vs. Ω_M plane.

where n_e is the free electron density and σ_T is the Thomson cross-section. The optical depth is here defined as a function of conformal time, such that $\tau(\eta)$ is related to the fraction of the intensity that remains today over the initial intensity at η. The differential equation for τ as a function of our time variable x is

$$\tau' = \frac{d\tau}{dx} = -\frac{cn_e\sigma_T}{H}. \tag{11}$$

We define the free electron fraction as

$$X_e = n_e/n_H, \tag{12}$$

where n_H is the proton density. We assume no heavier elements. Using that the mass of a proton is approximately equal to the mass of hydrogen, m_H we get

$$n_H = \frac{\Omega_{b0}\rho_{c0}}{m_H a^3}. \tag{13}$$

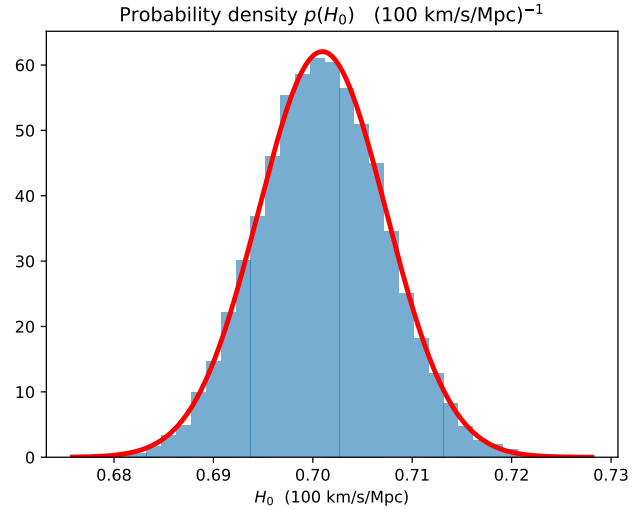

Fig. 8. The probability distribution of the Hubble parameter fitted with a Gaussian.

X_e can be solved in two different regimes. The first regime is when everything is in equilibrium, and the second regime is when the free electron fraction starts to decrease. The first regime is governed by the Saha equation given by

$$\frac{X_e^2}{1-X_e} = \frac{1}{n_b}\left(\frac{m_e T_b}{2\pi}\right)^{3/2} e^{-\epsilon_0/T_b}, \tag{14}$$

where $n_b = n_H$, m_e is the electron mass, T_b is the baryon temperature and ϵ_0 is the ionization energy of hydrogen. Since the Saha equation hold when photons and baryons are in equilibrium, the baryon temperature is equal to the photon temperature, T_{CMB}/a. The second regime is governed by the Peebles equation given below

$$\frac{dX_e}{dx} = \frac{C_r(T_b)}{H}\left[\beta(T_b)(1-X_e) - n_H\alpha^{(2)}(T_b)X_e^2\right], \tag{15}$$

where

$$\begin{aligned}
C_r(T_b) &= \frac{\Lambda_{2s\to1s}+\Lambda_\alpha}{\Lambda_{2s\to1s}+\Lambda_\alpha+\beta^{(2)}(T_b)}, \text{ (dimensionless)},\\
H &, \text{ (dimension } 1/\text{s)}\\
\Lambda_{2s\to1s} &= 8.227\text{s}^{-1}, \text{ (dimension } 1/\text{s)}\\
\Lambda_\alpha &= H\frac{(3\epsilon_0)^3}{(8\pi)^2 n_{1s}}, \text{ (dimension } 1/\text{s)}\\
n_{1s} &= (1-X_e)n_H, \text{ (dimension } 1/\text{m}^3)\\
n_H &= (1-Y_p)\frac{3H_0^2\Omega_{b0}}{8\pi G m_H a^3}, \text{ (dimension } 1/\text{m}^3)\\
\beta^{(2)}(T_b) &= \beta(T_b)e^{3\epsilon_0/4T_b}, \text{ (dimension } 1/\text{s)}\\
\beta(T_b) &= \alpha^{(2)}(T_b)\left(\frac{m_e T_b}{2\pi}\right)^{3/2} e^{-\epsilon_0/T_b}, \text{ (dimension } 1/\text{s)}\\
\alpha^{(2)}(T_b) &= \frac{64\pi}{\sqrt{27\pi}}\frac{\alpha^2}{m_e^2}\sqrt{\frac{\epsilon_0}{T_b}}\phi_2(T_b), \text{ (dimension m}^3/\text{s)}\\
\phi_2(T_b) &= 0.448\ln(\epsilon_0/T_b), \text{ (dimensionless)}.
\end{aligned}$$

where $\alpha \simeq \frac{1}{137.0359992}$. We now take transition rates between the 1s and 2s quantum states of the hydrogen atom.

The visibility function is given by $\tilde{g}(x) = -\tau' e^{-\tau}$.

Finally, the sound horizon is given by

$$s(x) = \int_0^a \frac{c_s dt}{a} = \int_{-\infty}^{x} \frac{c_s dx}{\mathcal{H}} \rightarrow \frac{ds(x)}{dx} = \frac{c_s}{\mathcal{H}}$$
$$\text{with } s(x_{\text{ini}}) = \frac{c_s(x_{\text{ini}})}{\mathcal{H}(x_{\text{ini}})}$$

where $c_s = c\sqrt{\frac{R}{3(1+R)}}$ where $R = \frac{4\Omega_{\gamma 0}}{3\Omega_{b0}a}$.

3.2. Implementation details

The code needs the background solution found in the previous milestone in order to run. The code solves the Saha and Peebles equations and calculates the optical depth and the visibility function. The differential equations are solved with a Runge-Kutta 4 ODE solver, and the result is splines using a cubic spline. We solve the quantities of interest from $x = -20$ until $x = 0$. We solve for 1000 points linearly spaced. We switch from the Saha equation to the Peebles equation when X_e reaches 0.99.

3.3. Results

3.3.1. Testing the code.

The code was mainly tested by comparing our plots to the plots of Winther (2023) and Callin (2006).

3.3.2. Our results

In figure 9 we see how the free electron fraction, X_e, evolves with time x. The blue plot is the free electron fraction using a combination of both the Saha and the Peebles equations. We see that before recombination, there were equally many free electrons as there were protons. Around recombination, we see that X_e has dropped to a tenth of its initial value, such that there are 10 times fewer free electrons at this time, using that the comoving proton density is constant. We aslo see that X_e seems to stabilize before it reaches 10^{-4}. The Saha prediction is plotted in orange. We see that the Saha equation predicts that X_e decreases more rapidly, and does not stabilize, but goes to zero. We see from the dotted line that recombination happens after X_e has started to decrease, which is consistent with intuition, as there must be fewer free electrons after atoms have started to form. The time of recombination was calculated using the visibility function, which we will discuss later.

In figure 10 we see the optical depth for photons emitted at time x received by us today. Since the optical depth tells us how the intensity of light decreases as it travels through a medium, we expect τ in general to be larger for larger x values as light has travelled a longer distance. We also expect τ to be larger if X_e is closer to one, since light scatters off free electrons. We clearly see that the optical depth is very large for photons that were emitted before recombination. After recombination, the universe became transparent. This is seen in the plot, as τ is several orders of magnitude lower after recombination, which means that photons emitted after recombination travelled mostly unimpeded. The reason why the optical depth decreases with x before recombination when X_e is constant is because light travels a shorter distance through the medium when x decreases. τ is obviously zero at $x = 0$ since there is no time for light to be scattered from $x = 0$ to $x = 0$. We see that τ is of order 10^4 at x=-12. This means that the observed intensity for light emitted at $x = -12$ is approximately a factor 10^{-4343} smaller than the initial intensity. Therefore, it is not possible, in a practical sense at least, to detect photons that were emitted before recombination.

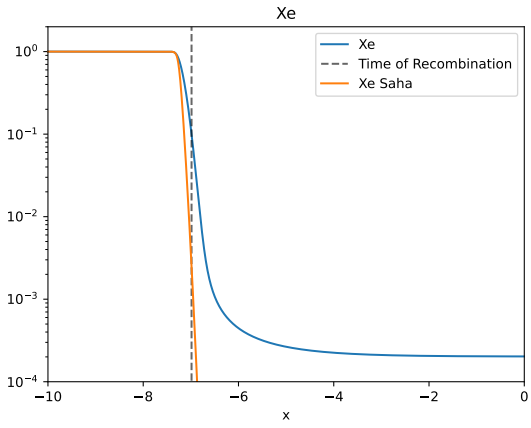

Fig. 9. The free electron fraction, X_e, plotted against x. The Saha prediction is also included in orange.

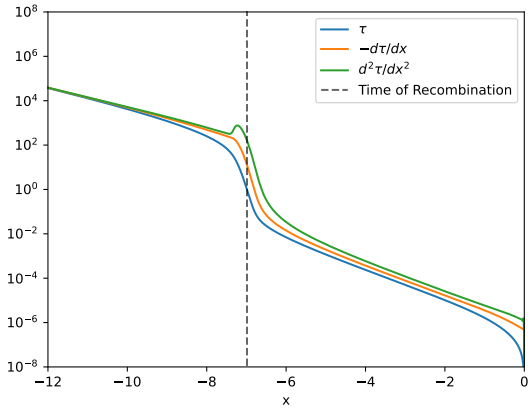

Fig. 10. The optical depth with its first and second derivatives are plotted against x.

In figure 11 we see the visibility function. Since the visibility function tells us the probability density that a photon scattered for the last time at x, the peak in the visibility function tells us the time when a photon was most likely to have scattered for the last time. By defining the last scattering surface to happen at this time, we get a value of $x = -6.98$ for the last scattering surface. The corresponding redshift is $z = 1079.73$ with cosmic time $t = 378004$ years. Recombination is the time when free electrons combined with protons to form hydrogen. This was possible since the photon temperature was, in general, too low to free the electrons by ionizing the hydrogen atoms. Recombination can therefore be defined when the abundance of free electrons reached a threshold value. We choose recombination to happen when the free electron fraction takes the value of

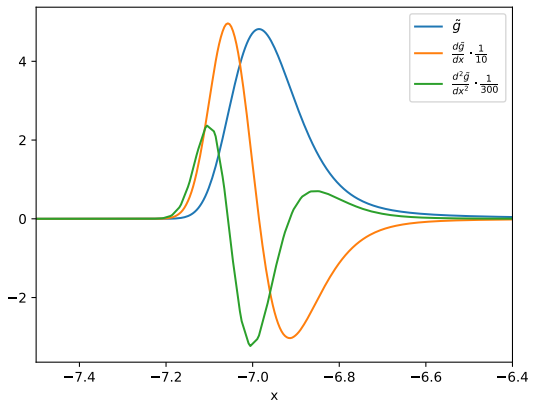

Fig. 11. The visibility function with its first and second derivatives are plotted against x.

0.1. Doing this we get exactly the same value of x as we did for the time of the last scattering surface. This reason why the values are exactly the same could be related to the splines, or to the resolution in x not being precise enough when extracting information from the arrays. Either way, this suggests that recombination happens very close to the last scattering surface. Knowing this, we can use the prediction of X_e from the Saha equation to give an estimate of both when recombination and the last scattering surface happened according to the Saha equation. Using $X_e = 0.1$ in the Saha equation we get that recombination happened at $x = -7.14$, $z = 1260$, $t = 290354$ years. From figure 9 we see that the Saha equation predicts that the free electron fraction drops more rapidly than the Peebles eqaution predicts. Recombination will therefore happen earlier using the Saha equation.

The free electron density today is $2 \cdot 10^{-4}$ meaning that for every two free electrons in the universe today, there are ten thousand protons. Since the comoving number density of protons is constant, we see that the free electron fraction can be rewritten into $\frac{n_{e\text{today}}}{n_{e\text{initial}}} = 2 \cdot 10^{-4}$, such that free electrons are five thousand times rarer today as they were initially, i.e. before recombination.

The sound horizon is the distance sound could have travelled in the proton-electron-photon plasma from the Big Bang until recombination, where the plasma ceases to exist. Since primordial energy density contrasts created sound waves in the plasma, and these sound waves froze as the plasma became neutral, we can expect to see those sound waves in the universe today. The sound horizon at recombination was 0.145 Gpc in comoving coordinates, i.e. in FLRW coordinates. To get the physical distance at any given time, we can multiply by the value of the scale factor at that time. Since we are only interested in physical distances today, we multiply by $a_0 = 1$, such that the physical distance of the sound horizon, at recombination, measured today is 0.145 Gpc. We therefore expect 0.145 Gpc to be the largest distances where the CMB is in equilibrium, since heat could not travel further than those distances. Therefore, people were surprised when CMB photons from the opposite sides of the universe appeared to be very close to equilibrium. This problem was solved by inflation.

4. Milestone III

In this milestone we calculate the evolution of the structures in the universe from after inflation until today. In practice, this is done by solving the perturbed Einstein-Boltzmann equations numerically with initial conditions from inflation. This will give us the time evolution of the different physical quantities we are interested in at different Fourier scales, k. We will go into more detail in the theory section. A detailed derivation of the relevant equations is given in Winther (2023).

The observed CMB is a measurement of the photon temperature field today. In order to reconstruct the statistical properties of the observations, we need to know how the structures in the universe evolved from some initial state to the state we observe today. This is important as matter perturbations will source gravitational wells that, by relativistic effects, will redshift the photons originating from inside the well. This will directly increase the photon temperature fluctuations that we are interested in.

4.1. Theory

Some regions in the early universe expanded more rapidly than others during inflation due to quantum fluctuations in the inflaton field, Winther (2023). These fluctuations made the energy density of the universe inhomogeneous, which introduced fluctuations in the famous Friedmann-Lemaître-Robertson-Walker (FLRW) metric. We can find the initial conditions for the metric perturbations, Ψ and Φ, in the Newtonian gauge, and from there find the initial conditions for the energy density perturbations of interest. This is done in Winther (2023).

The perturbations in the photon temperature field, δT, today are much smaller than the background temperature, $\overline{T}$. The same is true for the matter field on large scales. This suggests that we can apply linear perturbation theory on the distribution functions and expect that the result will be valid today. The perturbed distribution functions, f_i, for baryons, photons and CDM take the form

$$f_i(t, \boldsymbol{x}, \boldsymbol{p}) = \overline{f}_i(t, \boldsymbol{p}) + \delta f_i(t, \boldsymbol{x}, \boldsymbol{p}),$$

where $\overline{f}_i$ is the background distribution function and δf_i is the perturbation. These perturbations will of course perturb the energy momentum tensor in the Einstein equations, which in turn will perturb the metric. This will then change how particles move through space and time, Winther (2023). We will therefore have a system of coupled differential equations. The perturbed Einstein-Boltzmann equations can be solved in Fourier space with $x = \ln a$ as the time variable. The photon temperature perturbations, here defined as the relative perturbation $\Theta = \delta T/\overline{T}$, are expanded in Legendre multipoles, such that we are left with multipoles, Θ_ℓ of the photon distribution. Similarly, the CDM and baryon overdensities we solve for are defined as $\delta_{\text{CDM}} = \frac{\delta\rho_{CDM}}{\overline{\rho}_{CDM}}$ and $\delta_{\text{b}} = \frac{\delta\rho_b}{\overline{\rho}_b}$. The velocities are defined similarly, such that they are dimensionless. We do not solve the equations for polarization, and neutrino perturbations are not included.

The initial conditions:

$$\Psi = -\frac{2}{3}$$
$$\Phi = -\Psi$$
$$\delta_{\rm CDM} = \delta_b = -\frac{3}{2}\Psi$$
$$v_{\rm CDM} = v_b = -\frac{ck}{2\mathcal{H}}\Psi$$

Photons:

$$\Theta_0 = -\frac{1}{2}\Psi$$
$$\Theta_1 = +\frac{ck}{6\mathcal{H}}\Psi$$
$$\Theta_2 = -\frac{20ck}{45\mathcal{H}\tau'}\Theta_1$$
$$\Theta_\ell = -\frac{\ell}{2\ell+1}\frac{ck}{\mathcal{H}\tau'}\Theta_{\ell-1}$$

The photon equations:

$$\Theta_0' = -\frac{ck}{\mathcal{H}}\Theta_1 - \Phi',$$
$$\Theta_1' = \frac{ck}{3\mathcal{H}}\Theta_0 - \frac{2ck}{3\mathcal{H}}\Theta_2 + \frac{ck}{3\mathcal{H}}\Psi + \tau'\left[\Theta_1 + \frac{1}{3}v_b\right],$$
$$\Theta_\ell' = \frac{\ell ck}{(2\ell+1)\mathcal{H}}\Theta_{\ell-1} - \frac{(\ell+1)ck}{(2\ell+1)\mathcal{H}}\Theta_{\ell+1} + \tau'\left[\Theta_\ell - \frac{1}{10}\Theta_2\delta_{\ell,2}\right],$$

where $2 \le \ell < \ell_{\rm max}$

$$\Theta_\ell' = \frac{ck}{\mathcal{H}}\Theta_{\ell-1} - c\frac{\ell+1}{\mathcal{H}\eta(x)}\Theta_\ell + \tau'\Theta_\ell, \qquad \ell = \ell_{\rm max}$$

Cold dark matter and baryons:

$$\delta_{\rm CDM}' = \frac{ck}{\mathcal{H}}v_{\rm CDM} - 3\Phi'$$
$$v_{\rm CDM}' = -v_{\rm CDM} - \frac{ck}{\mathcal{H}}\Psi$$
$$\delta_b' = \frac{ck}{\mathcal{H}}v_b - 3\Phi'$$
$$v_b' = -v_b - \frac{ck}{\mathcal{H}}\Psi + \tau' R(3\Theta_1 + v_b)$$

Metric perturbations:

$$\Phi' = \Psi - \frac{c^2k^2}{3\mathcal{H}^2}\Phi + \frac{H_0^2}{2\mathcal{H}^2}\left[\Omega_{\rm CDM0}a^{-1}\delta_{\rm CDM} + \Omega_{b0}a^{-1}\delta_b + 4\Omega_{\gamma 0}a^{-2}\Theta_0\right]$$
$$\Psi = -\Phi - \frac{12H_0^2}{c^2k^2a^2}\left[\Omega_{\gamma 0}\Theta_2\right],$$

where $R = \frac{4\Omega_{\gamma 0}}{3\Omega_{b0}a}$. Some of these equations are numerically unstable early on, where the large value of τ' is multiplied by the small value of $(3\Theta_1 + v_b)$. This regime is known as the tight coupling regime, where the universe was opaque, and it can be related to time when the following three conditions hold simultaneously: $|\tau'| > 10$, $|\tau'| > 10 \cdot \frac{ck}{\mathcal{H}}$ and $x \le -8.3$. The unstable equations are rewritten below.

$$q = \frac{-[(1-R)\tau' + (1+R)\tau''](3\Theta_1 + v_b)}{(1+R)\tau' + \frac{\mathcal{H}'}{\mathcal{H}} - 1} - \frac{-\frac{ck}{\mathcal{H}}\Psi + (1 - \frac{\mathcal{H}'}{\mathcal{H}})\frac{ck}{\mathcal{H}}(-\Theta_0 + 2\Theta_2) - \frac{ck}{\mathcal{H}}\Theta_0'}{(1+R)\tau' + \frac{\mathcal{H}'}{\mathcal{H}} - 1}$$
$$v_b' = \frac{1}{1+R}\left[-v_b - \frac{ck}{\mathcal{H}}\Psi + R(q + \frac{ck}{\mathcal{H}}(-\Theta_0 + 2\Theta_2) - \frac{ck}{\mathcal{H}}\Psi)\right]$$
$$\Theta_1' = \frac{1}{3}(q - v_b').$$

The $2 \le l$ photon multipoles in the tight coupling regime are given by the same expressions as in the initial conditions, but these multipoles are very small in this regime, so we can simply set them to zero, but we choose to calculate the Θ_2 multipole for higher accuracy.

4.2. Implementation details

We solved the differential equations in two different regimes and "sewed" the solutions together. Since the last value in the first regime was used as an initial condition for the second regime, we removed the last value in the first regime, when "sewing" the solutions together, to remove the overlap between the solutions. A for loop was used to loop through all the Fourier scales, k, of interest. The differential equations were solved using a Runge-Kutta 4 ODE solver. The solution was then splined with a 2D spline, since we have a complete solution in time for each k value.

Solutions of the background universe and the recombination history of the universe was also used. We solved the system from x=-20 to x=0 with 1000 linearly spaced points. The k/Mpc values range from $5 \cdot 10^{-5}$ to 0.3 with 100 logarithmically spaced points.

4.3. Results

4.3.1. Test results

The code produces the following results with the cosmological test parameters given in table 2. All the figures show plots at three different scales. In figures 12 and 13 we see the density perturbation and the velocity, respectively, for both CDM and baryons. In figures 14 and 15 we see the photon temperature monopole, Θ_0, and the photon temperature dipole, Θ_1, respectively. The gravitational potential, Φ, is plotted in figure 16. All plots seem to agree with the plots shown in Winther (2023).

Table 2. Cosmological test parameters.

Parameter	Value
h	0.7
$\Omega_{\rm b}$	0.05
$\Omega_{\rm CDM}$	0.45
Ω_Λ	0.5
$\Omega_{\rm k}$	0
Ω_ν	0
$T_{\rm CMB}$	2.7255 [K]

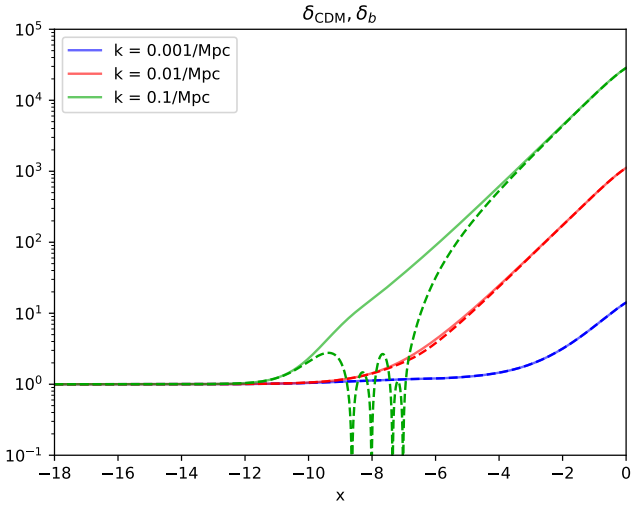

Fig. 12. The CDM overdensity, in solid lines, and the absolute value of the baryon overdensity, in dotted lines, are plotted at different scales, k.

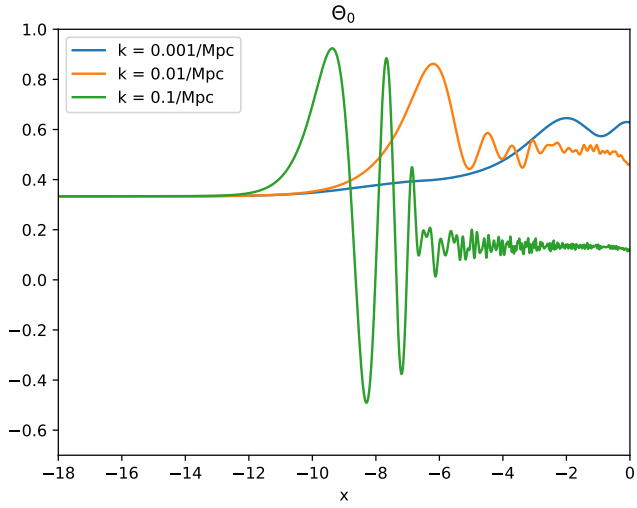

Fig. 14. The photon temperature monopole, Θ_0, at different scales, k.

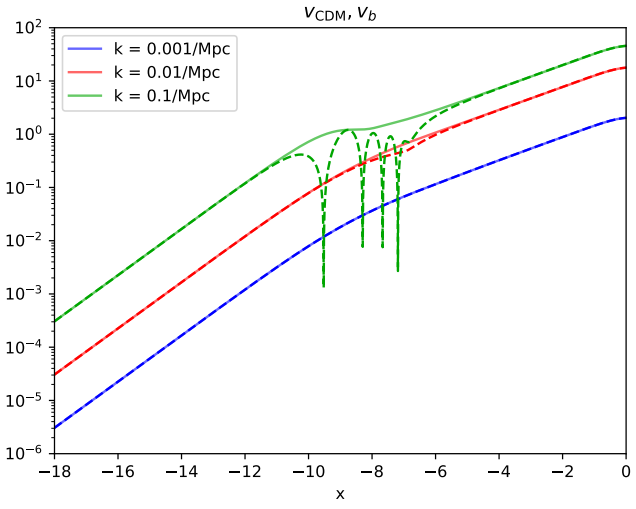

Fig. 13. The CDM velocities, in solid lines, and the absolute value of the baryon velocities, in dotted lines, are plotted at different scales, k.

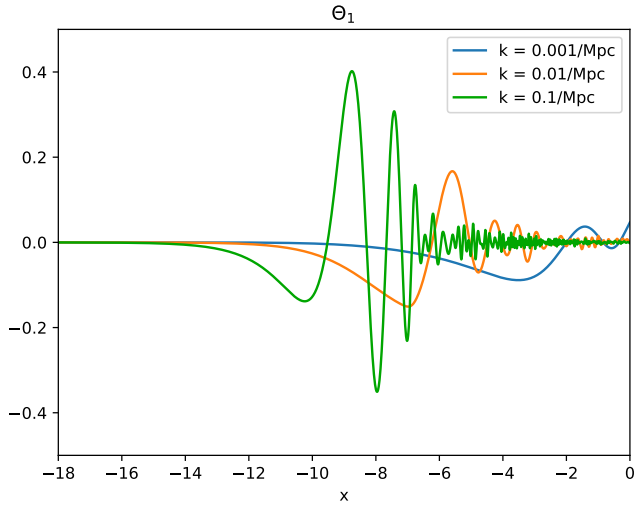

Fig. 15. The photon temperature dipole, Θ_1, at different scales, k.

4.3.2. Results

For our results we have again used the fiducial cosmology parameters of Winther (2023), but we removed the neutrinos from the background. Since we do not perturb the neutrinos, we believe including them in the background would be inconsistent. We also noted that the results we got with neutrinos included did not agree with CMB observations.

In figure 19, which is a zoomed in version of figure 18, we see more clearly what is going on. Gravity travels with the same speed as light. This means that the conformal time, η, gives us the maximum reach of gravity at any given time. Therefore, if the scale, k, of interest is larger than the conformal time, we should not see any correlation, since the scale is causally disconnected. Using that Fourier modes enter the particle horizon when $k\eta = 1$, we find that the scale $k = 10/\text{Mpc}$ enters the particle horizon at $x \sim -15.4$. We see that our results are consistent with the theory, as CDM clusters on this scale at $x \sim -16$. The reason why the baryonic overdensity oscillates, is because the mass is first compressed by gravity, then the radiation pressure increases such that the mass rebounds, as seen in figure 20. This process is then repeated until the Jeans mass is reached, where the Jeans mass is the mass needed to form structure. Since the Jeans mass, in a static universe, depends linearly on the sound speed, we do not expect baryon structure to form in general before recombination, where the sound speed was $\sim c$, Shen (2022). However, right after recombination the sound speed freezes out, i.e. the photons pressure is released, and structures can more easily form. As recombination happened at $x \sim -7$, we can see in our results that the baryon overdensity starts to continously increase at this time for scales that have entered the horizon. For CDM we do not have any oscillating behavior at early times since CDM is pressureless and gravity only has to works against the cosmic

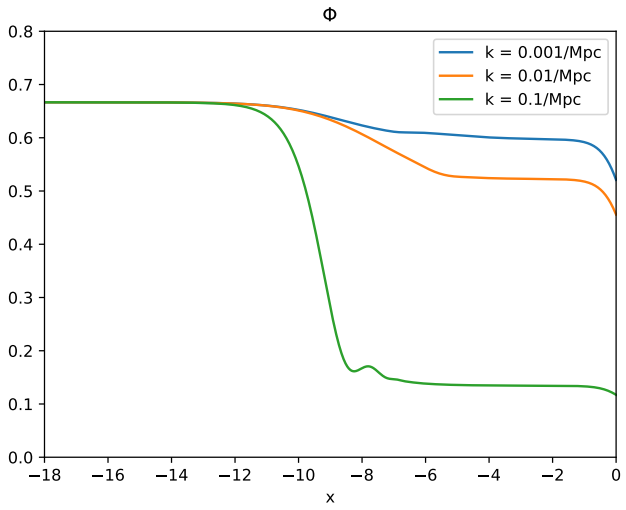

Fig. 16. The gravitational potential, Φ, at different scales, k.

acceleration. We note that the overdensity at some times is less than -1, which by definition is impossible in real space. This is not a concern, since the quantities are in Fourier space, and they have not been scaled to represent physical values.

In figure 22 we see that the oscillations in the baryonic overdensity has an expected corresponding oscillation in the baryonic fluid velocity, as the mass is contracting and rebounding repeatedly. At a larger scale, seen in green, the mode enters the particle horizon later, and the baryonic overdensity undergoes fewer oscillation. For even larger scales, seen in red and blue, the modes enter the particle horizon after recombination and there are no oscillations as expected.

In figure 17 we see how the temperature overdensity behaves for different scales. The corresponding oscillations in the photon fluid velocity can be seen in figure 21. At early times, the photons interact strongly with the baryons, such that they equilibrize. This is clearly seen in figure 20. After recombination, the photons will no longer follow the evolution of the baryons. This is because the baryons cluster more and more due to gravity, while photons do not. We see from the orange graph in 17 that the temperature overdensity increases as the scale enters the horizon and the evolution follows that of the baryons. However, at recombination, the pressure is released, so the temperature does not increase again with the baryons as we observe for smaller scales that enter the horizon at earlier times. Since the orange graph, with $k = 0.01/Mpc$ is large at recombination, we expect there to be strong correlation in the CMB power spectrum at these comoving scales, since it is the photons released at recombination we observe today. We note that the photon overdensity in the blue graph, with $k = 0.001/Mpc$ which enters the horizon later, also increases with the baryon overdensity even after recombination when the photons have decoupled from the baryons. This may suggest that there are still some interactions between the photons and the baryons. Another explanation is seen from figures 24 and 25 where the gravitational potentials are plotted. We see that for large scales at late times, the potentials are at their largest value. This may explain why the photons cluster even after recombination, since general relativity predicts that light is affected by the gravitational potential.

The evolution of the gravitational potential in **??** is clearly dependent on when the scale crosses the horizon, and if the crossing happens in the radiation era or in the matter era. In the radiation era, the photon perturbations will be the dominant quantity that can affect the potential. Since the photon perturbations do not grow in time, the potential will be washed out due to the expansion of the universe. This is clearly observed in the plot, as the scales that enter in the radiation era starts to decrease as they cross the horizon. For the scales that enter in the matter era, the evolution is quite different. Inside the matter era, the dominant quantity to affect the potential is the matter perturbations. We know that the matter perturbations grow in the matter era, and it can be shown analytically that the potential will be constant, but it takes some time before the universe becomes matter dominated after radiation-matter equality. We note that the $k = 0.001/Mpc$ scale is the only scale where Φ decreases before it enters the horizon. The fact that the potential changes before horizon crossing is unexpected, and should be explored in future studies. At very late times, the potential decreases again due to dark energy, which washes out the potential through more rapid expansion.

In figure 25 we see that the sum of the potentials are large for large scales at late times. The potential Φ in the Newtonian gauge can be related to the Newtonian gravitational potential. We see that during the matter era, there is a strong potential at large scales.

In figure 23 we see the photon quadrupole, which is analogous to a higher order Taylor expansion term. This term will therefore tell us about the finer structure of the photon temperature fluctuations. Since the observed CMB is a measurement of the photon temperature fluctuations that originate from the universe at recombination, $x \sim -7$, we can expect there to be correlation at scales corresponding to $k = 0.1/Mpc$. The larger scale, $k = 0.001/Mpc$, is very small and flat at this time, so we should not expect to see correlations at these scales.

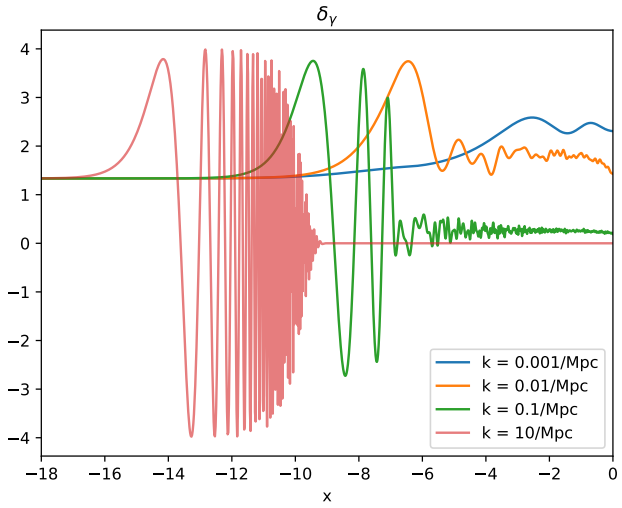

Fig. 17. The comparable photon overdensity, $\delta_\gamma = 4\Theta_0$, at four different scales, k.

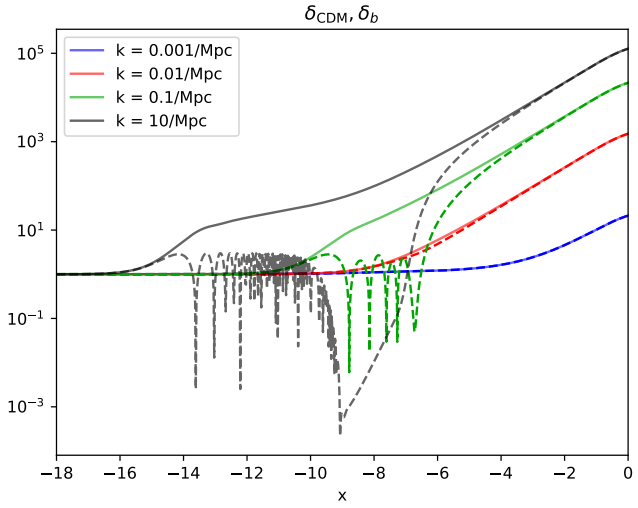

Fig. 18. The CDM overdensity and the absolute value of the baryon overdensity plotted at four different scales, k. The solid lines are for CDM and the dotted lines are for baryons.

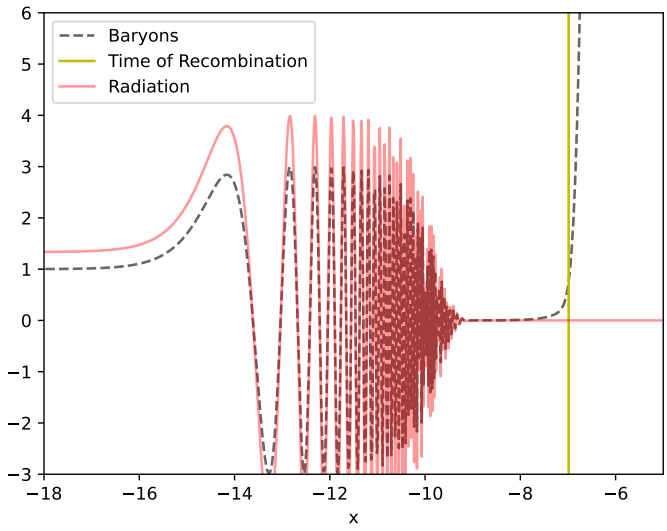

Fig. 20. Same as figure 19 at $k = 10/Mpc$ with radiation overdensity included.

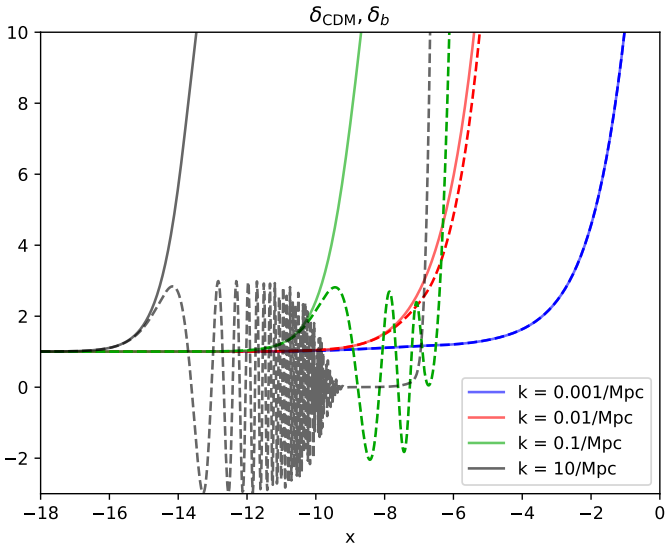

Fig. 19. A closer look at figure 18 with linear y-scale and with the correct sign for the baryon overdensity.

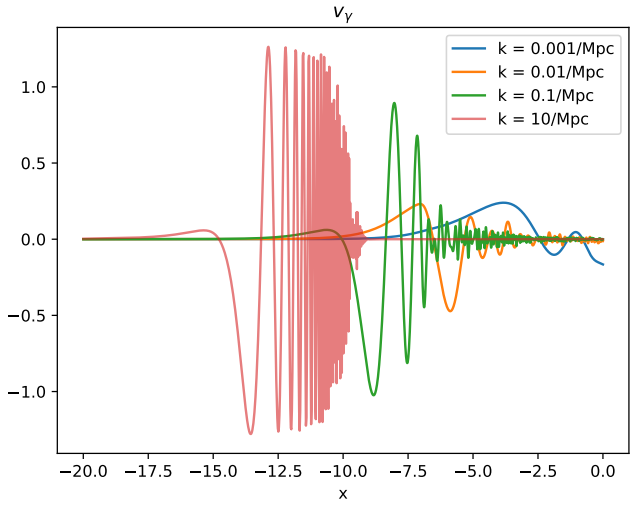

Fig. 21. The photon velocity perturbation, $v_\gamma = -3\Theta_1$, at four different scales, k.

5. Milestone IV

The perturbations we solved in the previous milestone are necessary in order to calculate what we should expect the universe to look like here and now. Since the only way of observing the universe is by changing the angle of observation today, we must calculate the angular dependency of the photon temperature field evaluated today. The transformation between scale, k, and direction, n, is through the spherical harmonics. The goal is therefore to have all the photon multipoles evaluated at all scales today, then transform this quantity such that we can recreate observations.

5.1. Theory

The CMB power spectrum, C_ℓ, is defined as

$$C_\ell \equiv \langle |a_{\ell m}|^2 \rangle = \langle a_{\ell m} a^*_{\ell m} \rangle, \tag{16}$$

where a_{lm} are the coefficients of the spherical harmonics used to transform the CMB temperature field. In principle, it is possible to get the C_ℓs by evaluating $\Theta_\ell(k, x = 0)$ and Fourier transform the coefficients back to real space, Winther (2023). However, as we are interested in ℓ values from $\sim 10^0$ to $\sim 10^3$, this approach would be very slow since we would have to solve thousands of coupled differential equations in the previous milestone. Instead, we can use the line of sight integral given below to calculate

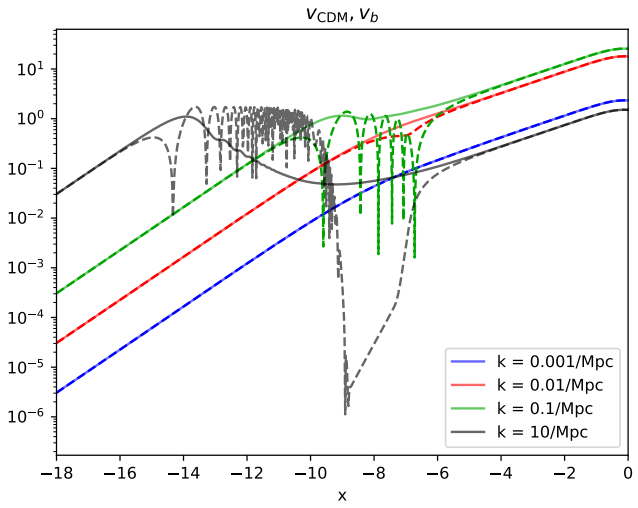

Fig. 22. The CDM velocities, in solid lines, and the absolute value of the baryon velocities, in dotted lines, are plotted at four different scales, k.

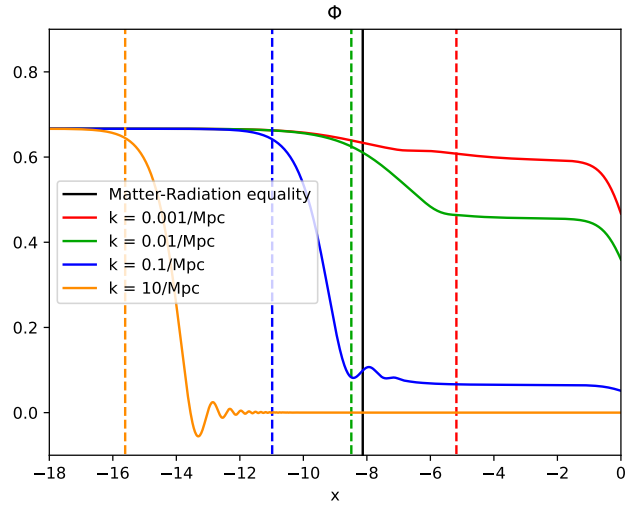

Fig. 24. The gravitational potential at four different scales, k. The dotted line denotes the time of horizon crossing for the scale with the same color.

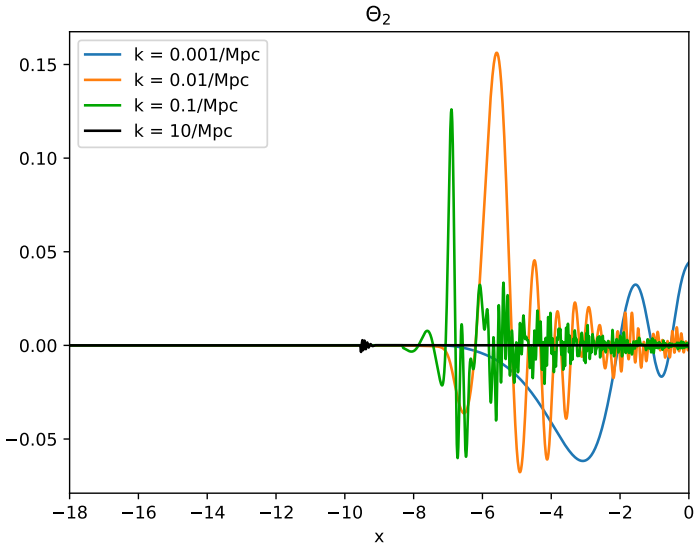

Fig. 23. The photon temperature quadrupole, Θ_2, at four different scales, k.

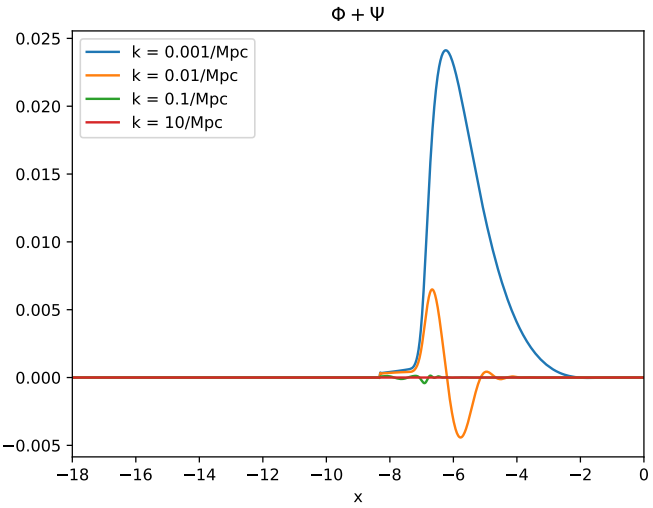

Fig. 25. The sum of the two gravitational potentials, Φ and Ψ, at four different scales, k.

$\Theta_\ell(x = 0, k)$ for arbitrary ℓ.

$$\Theta_\ell(k, x = 0) = \int_{-\infty}^{0} \tilde{S}(k, x) j_\ell[k(\eta_0 - \eta)] dx, \tag{17}$$

where the source function is defined as

$$\tilde{S}(k, x) = \tilde{g}\left[\Theta_0 + \Psi + \frac{1}{4}\Theta_2\right] + e^{-\tau}\left[\Psi' - \Phi'\right] - \frac{1}{ck}\frac{d}{dx}(\mathcal{H}\tilde{g}v_b) + \frac{3}{4c^2k^2}\frac{d}{dx}\left[\mathcal{H}\frac{d}{dx}(\mathcal{H}\tilde{g}\Theta_2)\right]. \tag{18}$$

$j_\ell(y)$ is the spherical Bessel function. The source function can be understood qualitatively. The first term is the photon monopole and the potential scaled by the visibility function evaluated along the line of sight. The potential will redshift the photons, as they climb out of the gravitational well. The second term is the Integrated Sachs-Wolfe (ISW) effect, which accounts for how the potentials change during the different eras. The third term is a Doppler term and the fourth term comes from scattering Winther (2023).

The CMB power spectrum can now be expressed as

$$C_\ell = \frac{2}{\pi}\int k^2 P_{\text{primordial}}(k)\Theta_\ell^2(k) dk, \tag{19}$$

which can be written as

$$C_\ell = 4\pi \int_0^\infty A_s \left(\frac{k}{k_{\text{pivot}}}\right)^{n_s - 1} \Theta_\ell^2(k)\frac{dk}{k} \tag{20}$$

by using a Harrison-Zel'dovich primordial power spectrum Winther (2023).

The matter power spectrum is defined by

$$P(k, x) = |\Delta_M(k, x)|^2 P_{\text{primordial}}(k), \tag{21}$$

where $\Delta_M(k, x) \equiv \frac{c^2 k^2 \Phi(k,x)}{\frac{3}{2}\Omega_{M0} a^{-1} H_0^2}$.

5.2. Implementation details

The code uses the results from the previous milestones, and the only new input parameters are the three parameters in the Harrison-Zel'dovich spectrum for the primordial power spectrum. We made some new splines needed for the source function by using the built-in methods for getting the derivative and the double derivative of a spline. When performing the line of sight integration, we used the trapezoid rule, with a variable step length as proposed by Callin (2006). However, this resolution was not fine enough, so we changed it for different ranges of ℓ. The k range where the integrand was highly non-zero was also dependent on ℓ. Of this reason, we made several ranges of different ℓ values where a specific k array would be used. This was done to reduce computation time as we encountered problems when splining the Bessel functions. The k ranges are called

```
n_k_zone_i,
```

where i runs from zero to five. The details are found in the PowerSpectrum.h file. The ranges for the ℓ values are listed below. $\ell <= 10$, $10 < \ell <= 30$, $30 < \ell <= 100$, $100 < \ell <= 300$, $300 < \ell <= 700$ and $\ell > 700$.

The C_ℓ integral is solved using the trapezoid rule with the substitution $dk \to d \log k$ with a variable step length.

The source function is calculated using k values linearly spaced from $5 \cdot 10^{-5}$/Mpc to 0.3/Mpc with 100 points. The x values range from $x = -10$ to $x = 0$ with 1000 linearly spaced points. The result was splined with a 2D spline.

5.3. Results

5.3.1. Test results

In figures 26 and 27 we have plotted the plots shown in Winther (2023) under "testing your code". We see that the CMB power spectrum has the same shape, but the values are too large. The same can be said about the matter power spectrum. This suggests that our results will in general be too large. There can be many reasons for this discrepancy, but we believe the error comes either from the calculation of the source function, or from an early k cut-off for the C_ℓ integration as we will discuss later.

5.3.2. Our results

In figures 28, 29, 30 and 31 we see some of the photon multipoles $\Theta_\ell(k)$ at $x = 0$. If we simply view the higher order photon multipoles as correction terms to the photon overdensity, we see that the photon overdensity corrections oscillate with respect to scale today. Since higher order photon multipoles correspond to higher order corrections, we expect the higher order multipoles to be small compared to lower orders, and relevant only at smaller scales, i.e. larger k. This is consistent with our results.

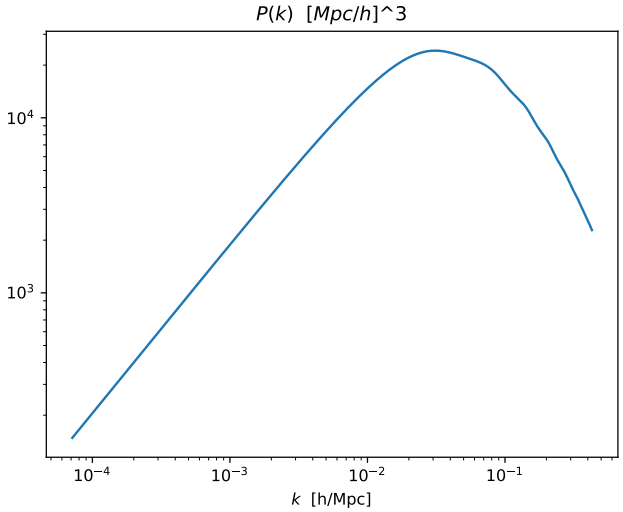

Fig. 26. The matter power spectrum with test parameters given by 2.

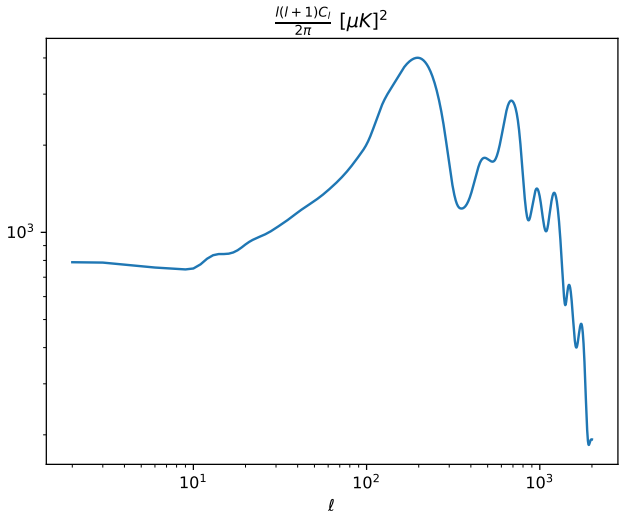

Fig. 27. The CMB power spectrum with test parameters given by 2.

We also observe that the oscillations are damped. This feature is most clearly seen in figure 31. One explanation for the damping is that at smaller scales, the photon perturbations are washed out due to photon scattering. Photon scattering is a process that naturally equilibrize the temperature such that perturbations are washed out. This effect is known as photon diffusion. Since all the plots are evaluated at today, there is no photon scattering anymore, but we still observe the result of the scattering that happened before recombination. The oscillations can therefore be viewed as old sound waves that have frozen out because the pre-recombination plasma, in which the waves propagated, does not exist anymore.

The k range in the plots is the range used in the integral in equation 20. We see that the cut-off in the k range seems too early. However, since we only need $\Theta_\ell{}^2$ the problem is not as serious. This is seen in figures 32 and 33. The cut-off exists only to reduce computation time. In figure 32 we clearly see that the

oscillations are asymmetric. This is because the cold dark matter component drives the overdensity such that the compressions become larger than it would have with baryons only. When the photon pressure decompresses the overdensity, the cold dark matter will slow down the expansion under gravity, and the decompression is reduced. This explains the asymmetry, but it is only a qualitative explanation, as we have not plotted the actual photon overdensity $\sim \Theta_0$.

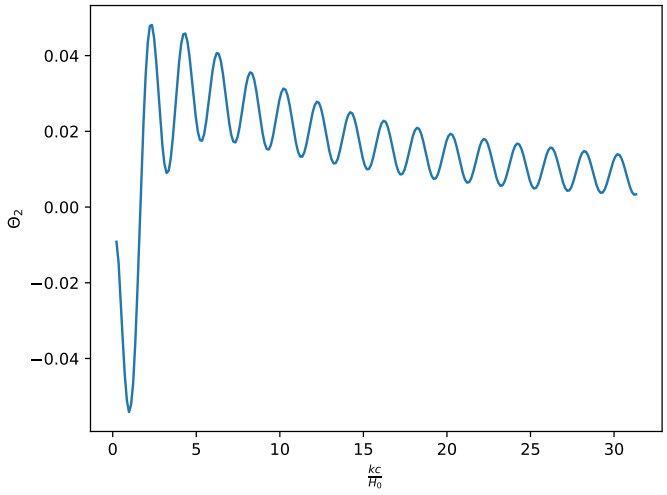

Fig. 28. The transfer function, $\Theta_2(k)$.

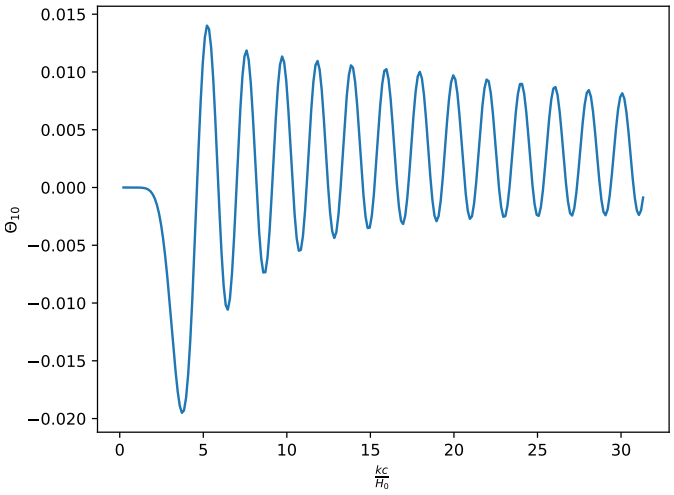

Fig. 29. The transfer function, $\Theta_{10}(k)$.

In figures 34, 35, 36 and 37 we see a part of the integrand in equation 20. All values are positive, and there is extra damping for large scales, as k is in the denominator. These plots are obviously closely related to the Θ_ℓs.

In figure 38 we show the matter power spectrum compared with results from other publicly available codes. The main difference between our result and the result from CLASS, Diego Blas (2011), is that we have not included neutrinos. The result from gevolution, J. Adamek & M. (2016), was obtained

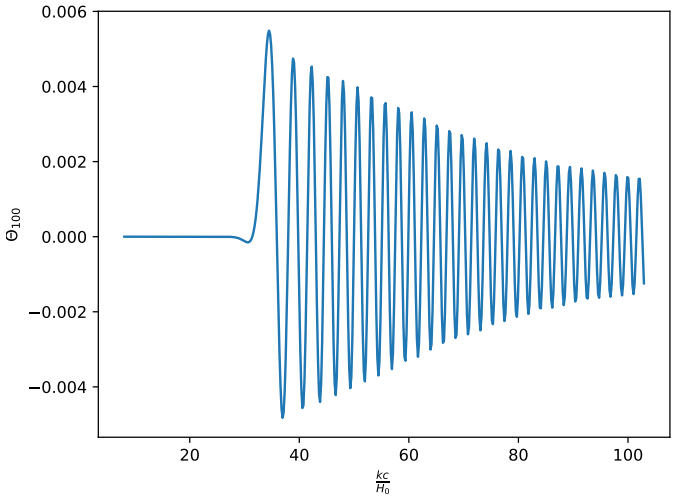

Fig. 30. The transfer function, $\Theta_{100}(k)$.

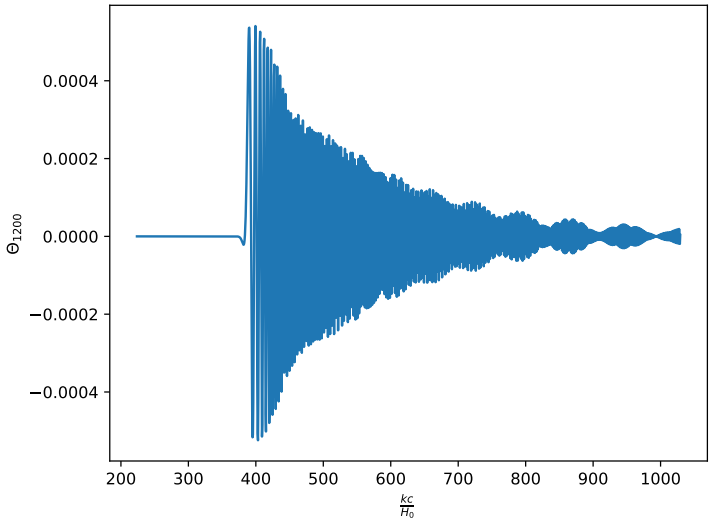

Fig. 31. The transfer function, $\Theta_{1200}(k)$.

from a dark matter simulation with relatively few particles, and is included here only to add credibility to our code. In figure 39 we have again plotted the matter power spectrum today, but we have also added data from observations. We again see that our matter power spectrum is too large. This is expected, as our test results indicated that our code produces too large values for both the matter and CMB power spectra. The most notable result is that the matter spectrum only grows up to some scale, k_{eq} entering the horizon at radiation matter equality, after which it starts to decrease. This can be understood from figure 24, where the potential, at scales entering the horizon before radiation matter domination, decreases drastically. This will suppress any matter perturbation, which in turn will suppress the power spectrum, since the power spectrum simply measures the strength of a perturbation on different scales. We also see that the potential remains much larger for scales entering the horizon after equality. This will lead to more power in the spectrum at these scales, as the matter will cluster more. Since

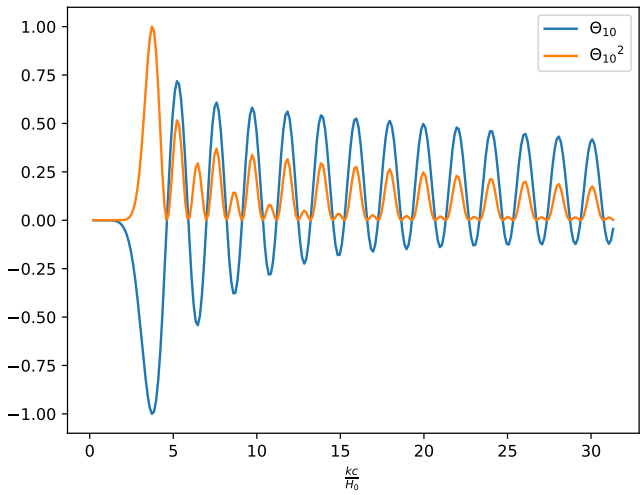

Fig. 32. The transfer function, Θ_{10} and its square both normalized to one.

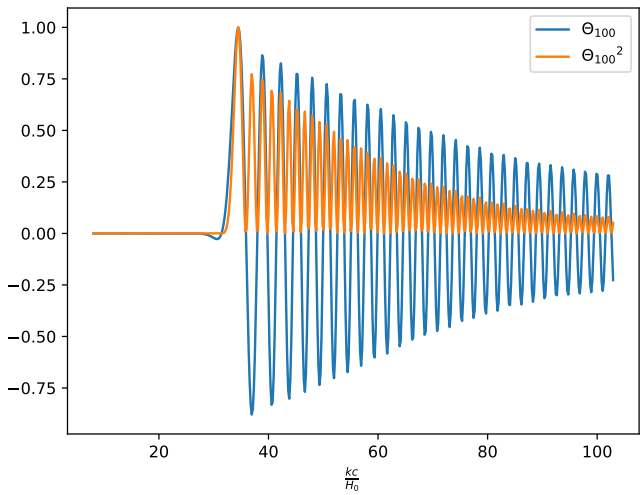

Fig. 33. The transfer function, Θ_{100} and its square both normalized to one.

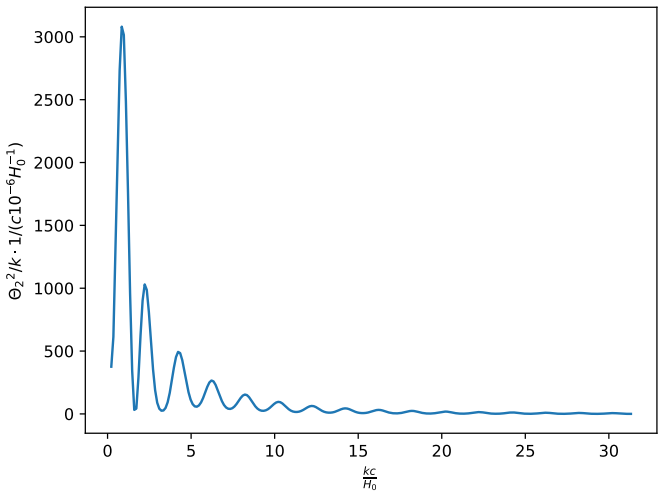

Fig. 34. The integrand of the C_2 integral.

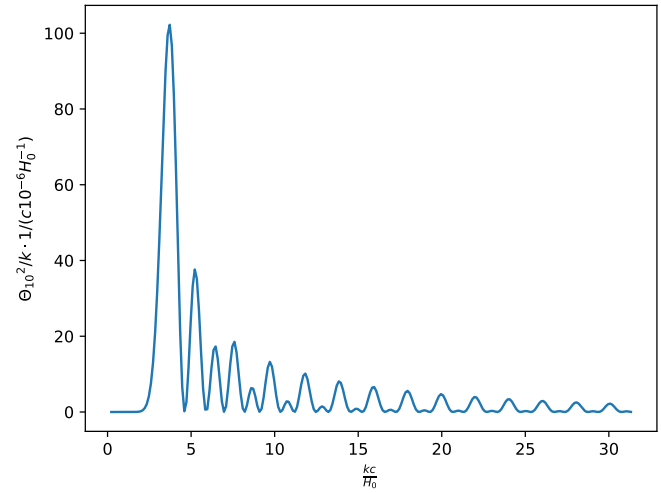

Fig. 35. The integrand of the C_{10} integral.

the perturbations also grow with time, we can not only look at the potential. For scales that entered the horizon at late times, the perturbations will be small relative to the scales that entered earlier, but later than equality. Therefore, for smaller and smaller scales that entered the horizon before equality, the perturbations are more and more suppressed by the decreasing potential, so the power spectrum decreases more and more. For scales larger that equality, the potential will be larger for larger scales, but these scales have little time to grow, so the largest perturbations today are those who entered the horizon at equality. Those entering after had less time to grow, so the power spectrum decreases for very large scales. This is observed in the power spectrum.

In figure 40 we see the CMB power spectrum with data overplotted. We observe that our result lies within the uncertainty at low ℓs. The reason why the uncertainty is large at low ℓ is because small ℓs correspond to large scales, and correspondingly fewer measurements. We have calculated the average CMB power spectrum over all universes, but we only live in exactly one, so there can be statistical variance. For large ℓ this uncertainty is suppressed as we use more measurements. We observe several peaks in the power spectrum. The first peak from the left is a compression, followed be a decompression seen in the second peak. The third peak is another compression and so on. These oscillations originate from the time before recombination when the plasma was oscillating back and forth due to gravity and radiation pressure. The reason why there are no peaks at larger scales, is that the sound waves did not have enough time to travel larger distances, as the plasma became neutral and ceased to exist at recombination. If recombination had happened later, the sound waves could have travelled larger distances, and the first peak would be located at larger scales. Since the large scales entered the horizon more recently, they would not have changes so much, and the power spectrum at

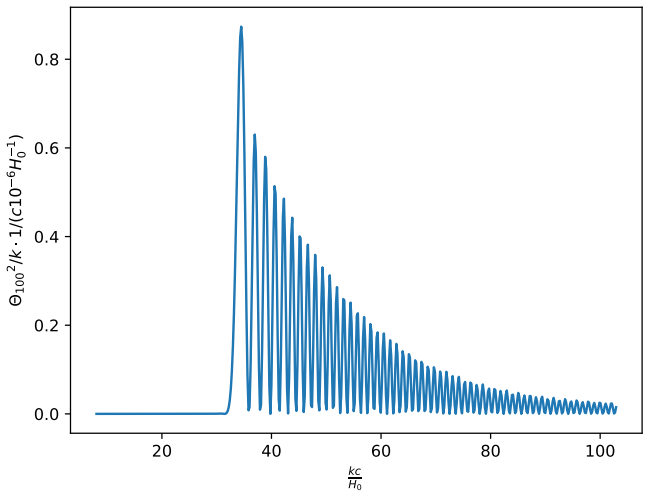

Fig. 36. The integrand of the C_{100} integral.

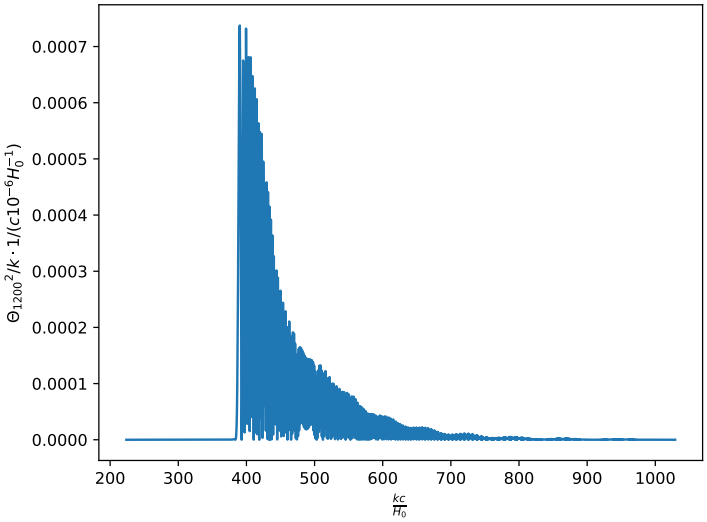

Fig. 37. The integrand of the C_{1200} integral.

these scales will be similar to the initial conditions. At small scales we clearly see the photon diffusion we discussed earlier.

6. Conclusions

We were able to calculate a CMB power spectrum in four steps. We started by calculating the evolution of the background universe in milestone 1. We found that the universe is 13.86 Gyr in cosmic time, which is consistent with modern science. In milestone 2 we calculated the recombination history of the universe. This was done by solving equations for the free electron density as a function of time. Our main result was that recombination happened at ca. 380 thousand years in cosmic time. This is also consistent with expectations. In the third milestone we calculated the evolution of perturbations in the background. Here we got many results, and they were mostly in agreement with expectations. Then, finally in milestone 4 we were able to put everything together using the line of sight integration. After the integral was calculated we could easily

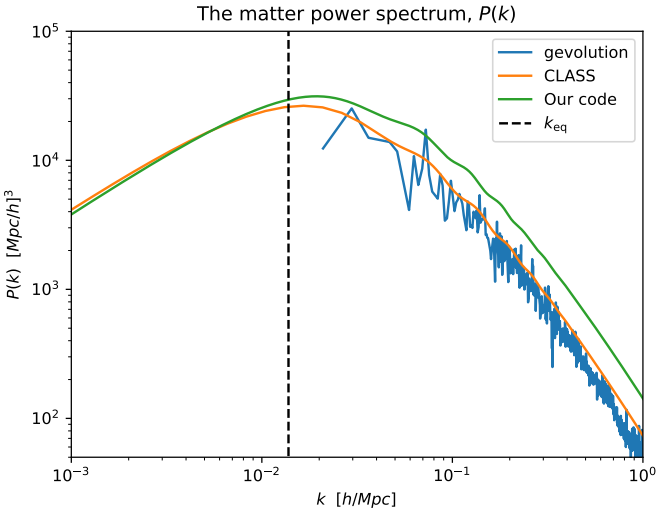

Fig. 38. The matter power spectrum compared to the result of publicly available codes CLASS(Boltzmann) and gevolution(relativistic N-body). CLASS was run with Planck cosmology and gevolution was run for dark matter.

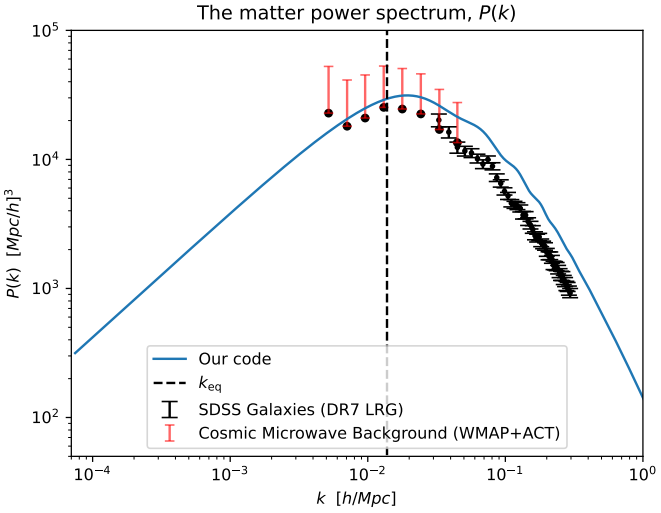

Fig. 39. The matter power spectrum with data. The uncertainty, in red, is only an upper bound.

calculate the CMB power spectrum. As expected, we observed several peaks corresponding to compressions and decompressions in the plasma that existed before recombination. Our results were more or less in agreement with observations.

Improvements can be done by including neutrinos and polarization. In addition, our code produces too large values for the power spectra and it is very slow. In order to improve accuracy, we should avoid taking the first and second derivatives of a spline, and use the correct analytical expressions especially when calculating the source function. The integrals in milestone 4 can be solved as a differential equation instead of using the trapezoid rule. In order to speed up the code the Bessel function should be splined. When we used the splined Bessel function we observed a phase shift with respect to the exact function.

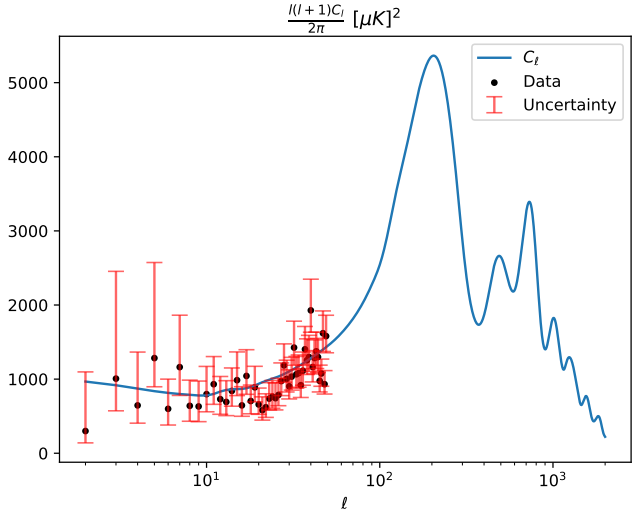

Fig. 40. The CMB power spectrum.

This was serious, since the error was located near recombination where several quantities change rapidly.

References

Callin, P. 2006, How to calculate the CMB spectrum
Diego Blas, Julien Lesgourgues, T. T. 2011, Journal of Cosmology and Astroparticle Physics (JCAP)
J. Adamek, D. Daverio, R. D. & M., K. 2016, Nature Phys. 12, 346
Scott Dodelson, F. S. 2021, Modern Cosmology, 2nd edn. (Academic Press)
Shen, S. 2022, AST4320: Cosmology and Extragalactic Astrophysics Lecture 1 - 2
Winther, H. A. 2023, Numerical Project and Lecture Notes